RESEARCH PAPER

Formulation and Evaluation of Novel Nilotinib loaded Photoluminescence Carbon Dots for Targeted Delivery of Anticancer Agent

[1]*Rampal Prem Jadhao, [2]V. N. Deshmukh

[1]Research scholar, Sudhakarrao Naik Institute of Pharmacy, Pusad, Maharashtra-445204

[2]Professor, Sudhakarrao Naik Institute of Pharmacy, Pusad, Maharashtra-445204

***Corresponding Author**

Rampal Prem Jadhao

Research scholar, Sudhakarrao Naik Institute of Pharmacy, Pusad, Maharashtra-445204

Email: rampaljadhao1995@gmail.com

Received: 25th Dec, 2025; Revised: 11th Feb 2026; Accepted: 22nd Feb, 2026; Available Online: 10th March, 2026

ABSTRACT

Poor medication solubility, low bioavailability, systemic toxicity, and lack of target specificity are frequently barriers to cancer treatment. A second-generation tyrosine kinase inhibitor with strong antitumor effects, nilotinib has inconsistent pharmacokinetics and poor water solubility. The goal of the current study was to create carbon dot-based nanocarriers functionalized with folic acid for better Nilotinib distribution and therapeutic efficacy. To create NF1–NF9 formulations, carbon dots were effectively synthesized, functionalized with folic acid, and loaded with nilotinib. Good colloidal stability was indicated by dynamic light scattering analysis, which verified nanoscale particle sizes between 6.22 and 12.3 nm, low polydispersity indices (0.121–0.394), and negative zeta potential values (–14.5 to –25.2 mV). Because of its highest drug concentration (96.37%), maximum encapsulation efficiency (88.27%), and smallest particle size (6.22 nm), NF5 was determined to be the optimal formulation. Successful drug encapsulation and drug integrity preservation were verified by FTIR and UV–visible spectroscopy. The results of SEM and TEM investigations showed spherical, evenly distributed nanoparticles with a smooth shape and little agglomeration. While XRD studies demonstrated partial to complete amorphization of Nilotinib within the carbon dot matrix, favoring improved dissolution, DSC analysis revealed an endothermic peak at about 238.31 °C, suggesting the creation of a new crystalline or co-crystal phase. The structural integrity was confirmed by Raman spectroscopy, which revealed distinctive Nilotinib peaks at around 1648, 1611, 1446, and 1308 cm^{-1}. According to in vitro release experiments, NF5 achieved 96.92% release in 12 hours, demonstrating sustained drug release. Studies on A549 cells' cytotoxicity showed that NF5 had more anticancer activity than pure nilotinib. Apoptotic cell death was confirmed by fluorescence imaging with Hoechst 33342 and Calcein-AM. All things considered, folic acid-functionalized carbon dots loaded with nilotinib are a promising nanocarrier technology for theranostic and targeted anticancer treatments.

KEYWORDS: Raman spectroscopy, folic acid functionalization, carbon dots, nilotinib, nanocarrier, targeted drug administration, apoptosis, and theranostics.

How to cite this article: Jadhao RP, Deshmukh VN. Formulation and evaluation of novel nilotinib loaded photoluminescence carbon dots for targeted delivery of anticancer agent. Int J Drug Deliv Technol. 2026;16(8s): 164-189; DOI: 10.25258/ijddt.16.8s.19

1. INTRODUCTION

Cancer remains one of the leading causes of mortality worldwide, significantly affecting global health and life expectancy. Although conventional treatment modalities such as surgery, radiotherapy, and chemotherapy have improved patient outcomes, their clinical effectiveness is often limited by systemic toxicity, poor tumor specificity, multidrug resistance, and low bioavailability of anticancer drugs. Chemotherapy, despite being widely used, frequently causes severe adverse effects and lacks selective targeting of cancer cells, highlighting the need for safer and more efficient therapeutic strategies. In this context, nanotechnology-based drug delivery systems (DDSs) have emerged as promising tools by enabling targeted drug delivery, controlled release, and improved pharmacokinetic profiles [1-4].

Nanomaterials, defined by at least one dimension in the 1–100 nm range, possess unique physicochemical and biological properties that make them suitable for biomedical applications. Nanoparticle-based DDSs can

enhance drug solubility, improve bioavailability, reduce off-target toxicity, and allow the co-delivery of multiple therapeutic agents [5]. Among these, carbon-based nanomaterials-particularly carbon dots (C-dots)-have attracted considerable attention due to their excellent biocompatibility, low toxicity, high water solubility, and intrinsic fluorescence. These features make C-dots highly suitable for theranostic applications, enabling simultaneous drug delivery and real-time imaging in cancer therapy [6, 7].

C-dots, typically less than 10 nm in size, can be classified into carbon quantum dots, graphene quantum dots, polymer carbon dots, and graphitic carbon nitride quantum dots, depending on their structure and surface chemistry [8, 9]. Their tunable optical properties arise from quantum confinement effects and can be modified through size control, heteroatom doping, or surface functionalization. C-dots can be synthesized using top-down or bottom-up approaches, including hydrothermal, solvothermal, and carbonization techniques [10-13].

Nilotinib, a second-generation BCR-ABL tyrosine kinase inhibitor used in chronic myeloid leukemia, suffers from poor oral bioavailability and high plasma protein binding, limiting its therapeutic effectiveness. Encapsulation of nilotinib into C-dot nanocarriers can improve solubility, enhance drug loading, reduce systemic toxicity, and enable fluorescence-based tracking of drug delivery [14–17]. This study focuses on the design and evaluation of C-dot-based nanocarriers for targeted nilotinib delivery, aiming to develop an integrated theranostic platform that advances precision cancer therapy [18-20].

2. MATERIALS AND METHODS

Nilotinib, an anticancer medication, citric acid (CA), soy lecithin, distilled water, Pluronic F127, folic acid, phosphate-buffered saline (PBS, pH 7.4), dialysis membrane (MWCO 1000 Da), deionized water, and methanol were all employed in this work. Unless otherwise noted, Cosmo Chem. Pvt. Ltd. and Solanki Enterprises provided all reagents, while Research Lab Fine Chem Industries, Mumbai (Solanki Enterprise, Pune) provided methanol. Analytical-grade compounds were all utilized without additional purification.

3. METHODS

Step 1: Carbon Dot Preparation

To optimize the amount of lecithin used for carbon dot (CD) synthesis, varying concentrations of lecithin (0.25 g, 0.5 g, and 0.75 g) were added to 0.1 g of citric acid. After the addition of 50 mL of deionized water, the mixture was subjected to microwave irradiation at 680 W. The resulting semi-solid product was subsequently diluted with 25 mL of deionized water and sonicated to obtain a uniform dispersion. The prepared samples were then analyzed for fluorescence emission and UV–visible absorption characteristics, and fluorescence properties were specifically evaluated following the microwave treatment.

Step 2: Pluronic F127 Carrier Loading

Pluronic F127 (polymeric micelle carrier): While stirring at 2000 RPM, gradually add the previously made CD dispersion. To promote self-assembly into CD-Pluronic nano complexes, keep shaking or sonicating for 30 to 60 minutes.

Step 3: Surface Functionalization with Folic Acid

Folic acid (FA) was conjugated to the CD-Pluronic nanocomplexes containing surface hydroxyl or amine groups. The reaction mixture was stirred overnight at room temperature to promote covalent coupling, enabling targeted functionalization of the nanocomplexes [21].

Table 1: DOE Recommended and Experimental Batches

Formulation code	Citric Acid (%)	Soya Lecithin (%)	Pluronic F127 (gm)	Folic Acid (gm)
F1	0.36	0.5	0.2345	0.5
F2	0.2	0.5	0.2345	0.5
F3	0.28	1.5	0.2345	0.5
F4	0.36	1	0.2345	0.5
F5	0.28	0.75	0.2345	0.5
F6	0.2	0.75	0.2345	0.5
F7	0.2	1	0.2345	0.5
F8	0.36	0.75	0.2345	0.5
F9	0.28	0.5	0.2345	0.5

4. CHARACTERIZATION OF CARBON DOTS

4.1 Particle Size, PDI, and Zeta Potential (Horiba Scientific)

Dynamic light scattering (DLS) was used to measure the carbon dot formulation's particle size in triplicate using a Malvern equipment (MAL1065494). At a temperature of 25°C and a scattering angle of 90°, measurements were made. The intensity profile was used to evaluate the obtained particle size analysis results. The synthesized carbon dots were appropriately attenuated (1:100) with milli-Q water prior to analysis [22].

4.2 FTIR

An FT/IR-4600 Type A spectrometer (Model No. F193061786) with an attenuated total reflectance (ATR) accessory was used to get Fourier transform infrared (FTIR) spectra. The ATR crystal was directly coated with a small number of carbon dot samples, which were then compressed using the pressure arm. Using 32 co-added pictures, spectroscopic data were obtained at a resolution of 4 cm^{-1} spanning the spectral range of 4000–400 cm^{-1}. Before every measurement, a background spectrum was gathered. To make comparison analysis easier, the spectra were first corrected for baselines and then normalized [23].

4.3 Spectroscopy in the UV

10 mg of the material was dissolved in 10 mL of distilled water to create a standard stock solution, which had a 1000 µg/mL concentration.

Make a 10 ppm solution from a 1000 µg/mL stock solution by diluting 100 µL of the stock solution with distilled water until the final volume is 10 mL. The stock solution was analyzed via UV spectrophotometry (Jasco V-630) [150] across a wavelength range of 200-800 nm [24].

4.4 SEM, or scanning electron microscopy

Scanning Electron Microscopy (SEM) (Carl Zeiss, supra55, Germany) was performed at the Central Instrumentation Facility (SPPU, Pune). The specimens' photomicrographs were taken at 10,000x magnification.Electron microscopy is employed to ascertain fracture morphology, surface topography, and texture. The surface morphology of the optimized batches was characterized [25].

4.5 Transmission Electron Microscopy (TEM) (JEOL, 2200FS)

Transmission electron microscopy (TEM) has been employed for the analysis of surface morphology. Transmission Electron Microscopy (TEM) The surface morphology of the optimized NF6 batch was characterized utilizing Transmission Electron Microscopy (TEM).

A few microliters of a diluted carbon dot solution from optimized batch NF6 were applied to a 300-mesh copper grid film coated with copper and subsequently air-dried at ambient temperature. Following complete desiccation, the sample was stained with a 2% (w/v) phosphotungstic acid solution, and excess stain was subsequently removed via filter paper. Furthermore, digital micrographs and Soft Imaging Viewer Software were employed to acquire the sample analyses and accompanying images [26].

5. Synthesis of CD-Nilotinib Complexes

To facilitate complex formation, 1 mL of a cyclodextrin (CD) solution (8 mg mL^{-1}) and 1 mL of a nilotinib solution (400 µg mL^{-1}) were mixed with phosphate-buffered saline (PBS) at pH 7.4 and stirred to obtain a final volume of 4 mL. The resulting solution was incubated for 24 hours at 24 °C under light-protected conditions with continuous agitation at 200 rpm using an orbital shaker (Crystal, China). After incubation, the solution was dialyzed against 40 mL of deionized water for 2 hours using a dialysis membrane with a molecular weight cut-off of 1000 Da to remove unreacted nilotinib and free cyclodextrin. The prepared nilotinib-cyclodextrin complex was finally stored at 4 °C in the absence of light until further experimental use [21].

Experimental Framework

Response surface methodology (RSM) based on a Quality by Design approach was employed using a central composite design with two independent variables at two levels. Nilotinib concentration (A) was studied at a low level of 400 µg/ml and a high level of 800 µg/ml, while stirring speed (B) was evaluated at a low level of 1000 RPM and a high level of 2000 RPM. The effects of these variables on drug content and entrapment efficiency (to be maximized) and particle size (to be minimized) were investigated, as summarized in Table 1.

Table 2: DOE Suggested and Experimental batches

Formulation code	Nilotinib (µg/mL)	Stirring speed (RPM)
NF1	600	1500
NF2	800	2000
NF3	800	1500

NF4	600	1000
NF5	600	2000
NF6	800	1000
NF7	400	1000
NF8	400	2000
NF9	400	1500

6. Evaluation and Results of Drug loaded Carbon dots

6.1 Zeta Potential and Particle Size in Dynamic Light Scattering

The CD solution was diluted and then added to a foldable capillary cell fitted with platinum electrodes in order to measure the zeta potential and particle size. After that, this cell was placed inside a Zetasizer Nano's sample receptacle (Malvern, England) for examination [26].

6.2 Content of Drugs

The drug content was established in order to evaluate the consistency and effectiveness of the drug's inclusion into the formulation. To guarantee full extraction, a precisely weighed sample containing a known quantity of medication was dissolved in an appropriate solvent or buffer. After removing undissolved particles with a filter or centrifuge (Eltek OC 2F), the clear filtrate was examined at 247 nm using a UV-visible spectrophotometer. The formula below was used to get the drug content (%) [27]:

Measured drug concentration divided by theoretical substance concentration and multiplied by 100 is the drug content (%).

6.3 Effective Encapsulation

The percentage of the medication that was successfully integrated into the formulation was measured using encapsulation efficiency (EE). The unbound drug in the supernatant was separated by centrifuging a defined amount of the produced formulation after it had been dissolved in an appropriate solvent or buffer. The amount of free drug was measured at 247 nm using a UV-visible spectrophotometer (Jasco V-630). After that, encapsulation efficiency was computed using the formula [28]:

Encapsulation Efficiency (%) is calculated by dividing Total Drug by Free Drug * 100.

6.4 Study of Drug Diffusion in Vitro

A Franz diffusion cell (DBK 210796) was used in the in vitro drug diffusion study. The dialysis membrane, having been pre-soaked in phosphate buffer (pH 7.4) overnight, was then positioned between the donor and receptor chambers. Phosphate buffer (pH 7.4) was added to the receptor compartment, which was kept at 37 ± 0.5 °C and constantly shaken at 100 rpm. A predetermined amount of the formulation was added to the donor compartment in accordance with a predetermined medication dosage. 1 mL samples were taken at predetermined intervals for up to 12 hours, and to maintain sink conditions, an equivalent volume of fresh medium was added. Following analysis of the samples using UV-visible spectrophotometry at 250 nm, the cumulative percentage of drug release was computed [29].

6.5 FTIR

An attenuated total reflectance (ATR) accessory on an FT/IR-4600 Type A spectrometer (Model No. F193061786) was used to perform FTIR analysis. The ATR crystal was directly covered with a little quantity of sample, which was then compressed with the pressure arm. 32 scans with a resolution of 4 cm^{-1} were used to record spectra in the 4000-400 cm^{-1} range. Each measurement was preceded by the recording of a background spectrum, and the resulting spectra were normalized and baseline corrected for comparison analysis [30].

6.6 DSC

To evaluate drug-excipient compatibility, Differential Scanning Calorimetry (DSC) was carried out utilizing a METTLER TOLEDO system. Samples (2–5 mg) were enclosed in aluminum pans and heated under nitrogen from 30 to 300 °C at a rate of 10 °C per minute. Melting points, glass transition temperatures, and any thermal events suggesting interactions or alterations in crystallinity were examined in thermograms [31].

6.7 Analysis of Raman

When examining a substance's vibrational patterns, the Raman spectrum is a useful instrument that can provide important details about its molecular structure, crystallinity, and other structural features. In this study, the Raman spectrum was obtained using an excitation wavelength of 785 nm for the synthesized carbon dots [32].

6.8 Spectroscopy using fluorescence

A spectrofluorometer was used to examine the optical characteristics of carbon dots (CDs) at room temperature. After being sonicated for ten minutes, aqueous CD dispersions were made and filtered through a 0.22 µm membrane. Excitation-dependent emission was evaluated by recording emission spectra in the 300-600 nm band at different excitation wavelengths (300-420 nm). Excitation spectra were obtained by monitoring emission at the maximum wavelength. PMT voltage was tuned and slit widths were fixed at 5 nm. Fluorescence stability was evaluated under continuous illumination, different pH (2-10) and ionic conditions. Data were analyzed for emission maxima, intensity and excitation-dependent shifts [32].

6.9 Quantum yield

The quantum yield of carbon quantum dots (CQDs) was determined using the slope method with quinine hemisulfate in 0.1 M sulfuric acid (Φ = 0.54) as a reference. UV–vis absorbance of five concentrations of CQDs and quinine sulfate was measured at 360 nm and 310 nm, respectively, and photoluminescence spectra were recorded at 450 nm using corresponding excitation wavelengths. The fluorescence intensities were plotted against absorbance, and the quantum yield was calculated using:

Qc =Qr (mc/mr)(η2 c/η2 r)

where QQQ is quantum yield, mmm is the slope, subscripts rrr and ccc refer to reference and CQDs, and ηc\eta_cηc and ηr\eta_rηr (both 1.33) are the refractive indices of the respective solvents [33].

6.10 Transmission Electron Microscopy (TEM)

Samples were analyzed using a Transmission Electron Microscope (TEM, 2200FS) at 200 kV to study morphology and particle size. A dilute suspension (0.1 mg/mL) was drop-cast (5 µL) onto a carbon-coated copper grid, negatively stained with 1% uranyl acetate for 30 s, blotted, and air-dried. TEM images were captured at various magnifications, and particle sizes were measured using ImageJ software [34].

6.11 XRD

The data acquired from XRD (Bruker D8 Advance Series 1) was employed to assess whether the newly formed compounds are crystalline or amorphous. The measurement conditions included target metals Cu, filter K, an applied voltage of 40 kV, and a current of 30 mA. Nilotinib was scanned over a two-degree range of 10–90 °C with a 0.2 °C phase scale [35].

7. EVALUATION AND CHARACTERIZATION OF CARBON DOT

7.1 Particle Size, PDI and Zeta Potential (Horbia Scientific)

Table 3: Particle Size, PDI and Zeta Potential of CF1-CF9

Formulation Code	Particle Size (nm)	PDI	Zeta Potential (mV)
F1	10.2	0.285	-23.4
F2	12.4	0.253	-21.8
F3	30.9	0.315	-14.5
F4	23.6	0.316	-19.8
F5	25.3	0.287	-20.4
F6	**8.5**	**0.121**	**-25.2**
F7	18.9	0.178	-18.2
F8	23.2	0.394	-23.4
F9	16.1	0.248	-21.2

Conclusion

The formulations (F1–F9) showed particle sizes ranging 8.5–30.9 nm, PDI values of 0.121–0.394, and negative zeta potentials from −14.5 to −25.2 mV, indicating nanosized, fairly uniform, and stable carbon dots.

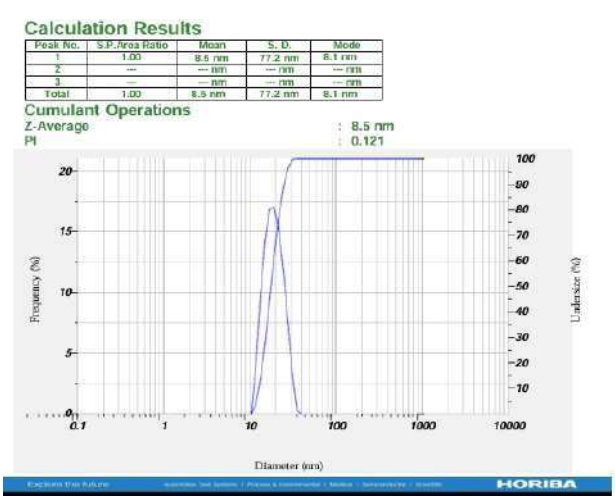

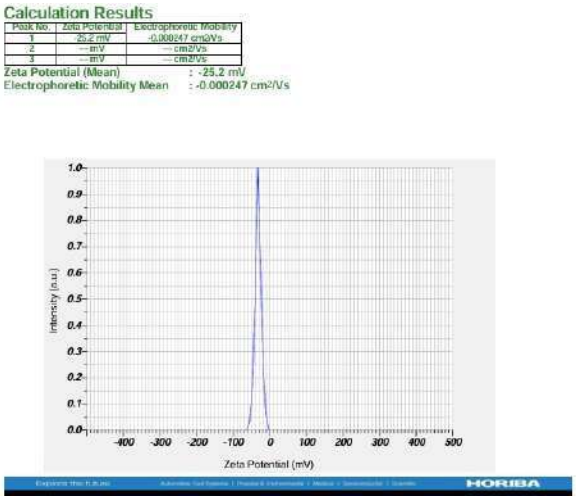

Fig 1 : Particle size of F6 **Fig 2: Zeta potential of F6**

ANOVA – Particle Size

The linear model for particle size is significant (F = 5.95, p = 0.0376). Soya Lecithin (B) significantly affects particle size (p = 0.0196), while Citric Acid (A) is not significant (p = 0.2150). The model explains 66.5% of the variability (R^2 = 0.6649) with good signal-to-noise ratio (adequate precision = 6.93), making it suitable for predicting particle size within the studied range.

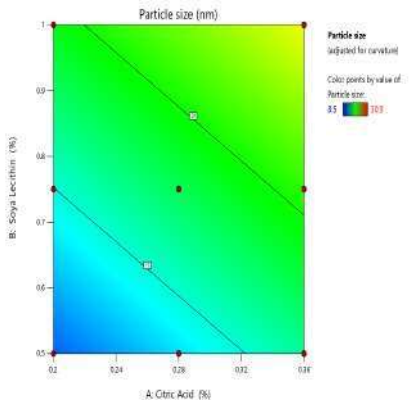

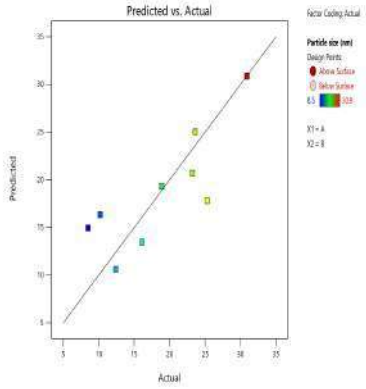

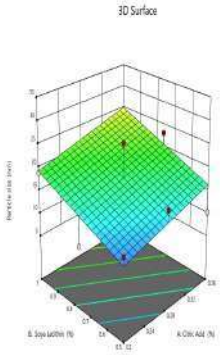

Fig 3: A **Fig 4: B** **Fig 5: C**

(Fig 5: Counter plot Fig 6: Predicted vs Actual plot Fig 7: 3D Surface plot)

ANOVA – PDI

The linear model for PDI is significant (F = 5.77, p = 0.0401). Citric Acid (A) significantly affects PDI (p = 0.0156), while Soya Lecithin (B) is not significant (p = 0.5680). The model explains 65.8% of the variability (R^2 = 0.6578) with good signal-to-noise ratio (adequate precision = 5.29), making it suitable for predicting PDI within the studied range.

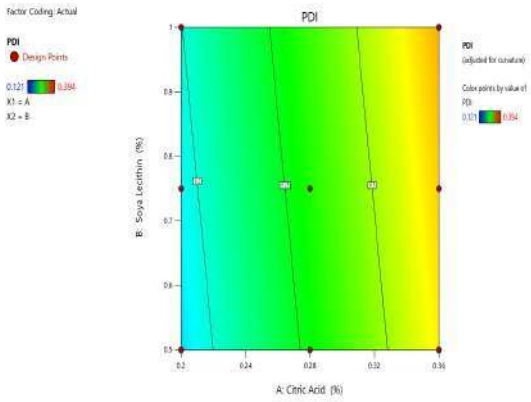

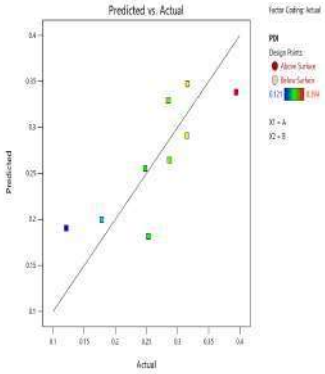

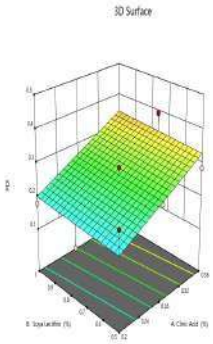

Fig 6: A **Fig 7: B** **Fig 8: C**

(Figure A: Counter Plot, Figure B: Predicted vs actual Plot, FigureC: 3D Surface Plot)

ANOVA – Zeta Potential

The linear model for zeta potential is significant (F = 5.48, p = 0.0442). Soya Lecithin (B) significantly affects zeta potential (p = 0.0164), while Citric Acid (A) is not significant (p = 0.8031). The model explains 64.6% of the variability (R^2 = 0.6464) with good signal-to-noise ratio (adequate precision = 6.40), making it suitable for predicting zeta potential within the studied range.

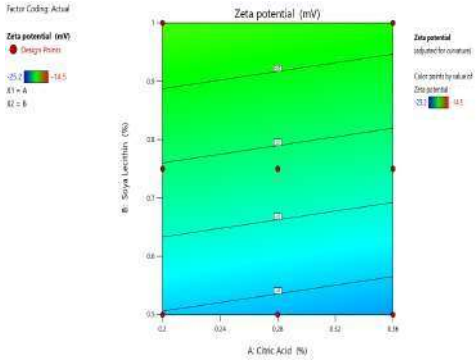

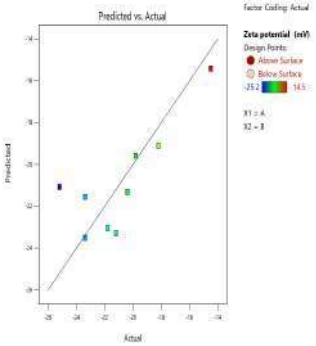

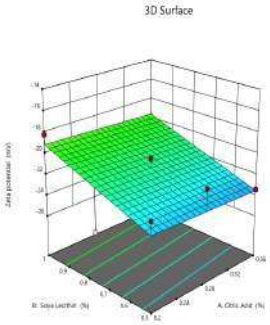

Fig 9: A **Fig 10: B** **Fig 11: C**

(Figure A: Counter Plot, Figure B: Predicted vs actual Plot, Figure C: 3D Surface Plot)

7.2 FTIR

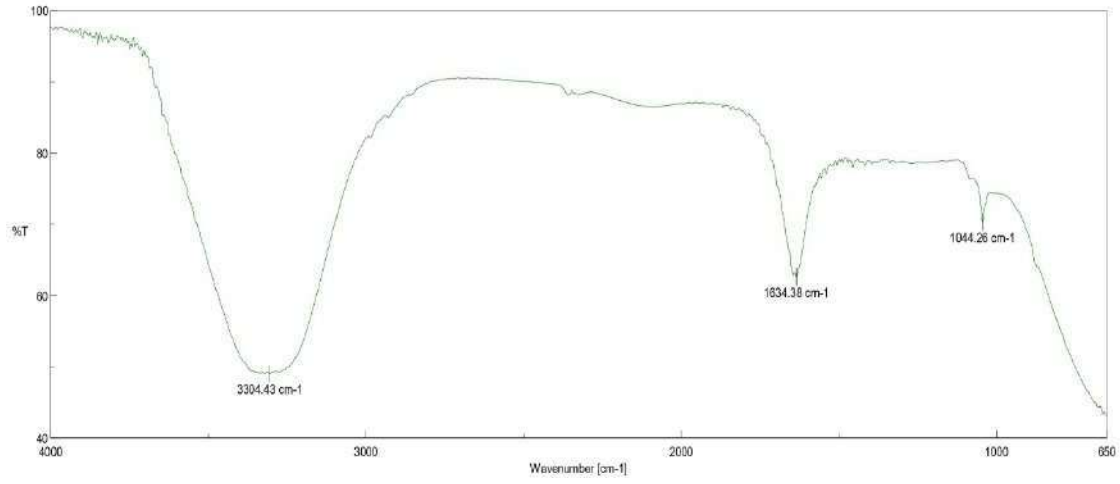

Fig 12: FTIR Spectrum of F6

Conclusion:

The FTIR spectrum shows a broad absorption band at around 3304.43 cm^{-1}, indicating the presence of N–H stretching vibrations characteristic of hydroxyl or amine groups, likely due to functional groups introduced during surface modification. The peak observed at 1634.38 cm^{-1} is attributed to C=O stretching, suggesting the presence of amide or carboxyl functional groups. Additionally, the 1044.26 cm^{-1} band is indicative of C–O or C–N stretching, confirming the incorporation of oxygen- and nitrogen-containing groups.

7.3 UV Spectroscopy

Table 4: UV Spectrum of F1-F9

Formulation	UV–Vis Absorption (nm)
F1	401
F2	401
F3	401
F4	401
F5	401
F6	401
F7	401
F8	401
F9	401

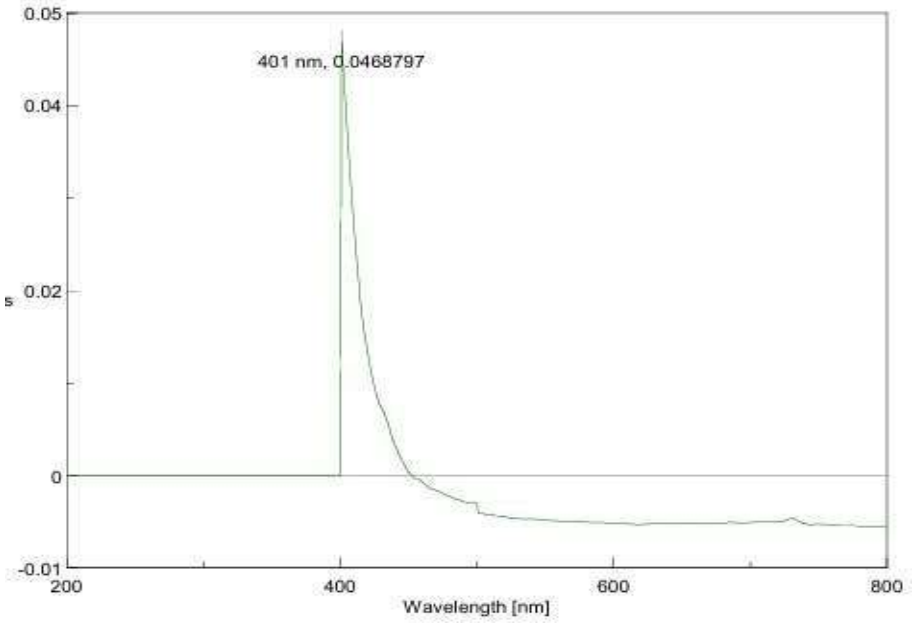

Fig 13: UV spectrum of F6

Conclusion

All the formulations NF1 to NF9 exhibited a characteristic UV–Visible absorption peak at 401 nm. The appearance of the absorption maximum at the same wavelength for all batches indicates that the chromophoric group of folic acid remains intact in each formulation and that there is no significant chemical interaction with the excipients such as citric acid, soya lecithin, or Pluronic F127. Hence, it can be concluded that all formulations (NF1–NF9) possess similar spectral characteristics, confirming the stability of folic acid and the absence of major chemical changes in the developed formulations.

7.4 Scanning Electron microscopy (SEM)

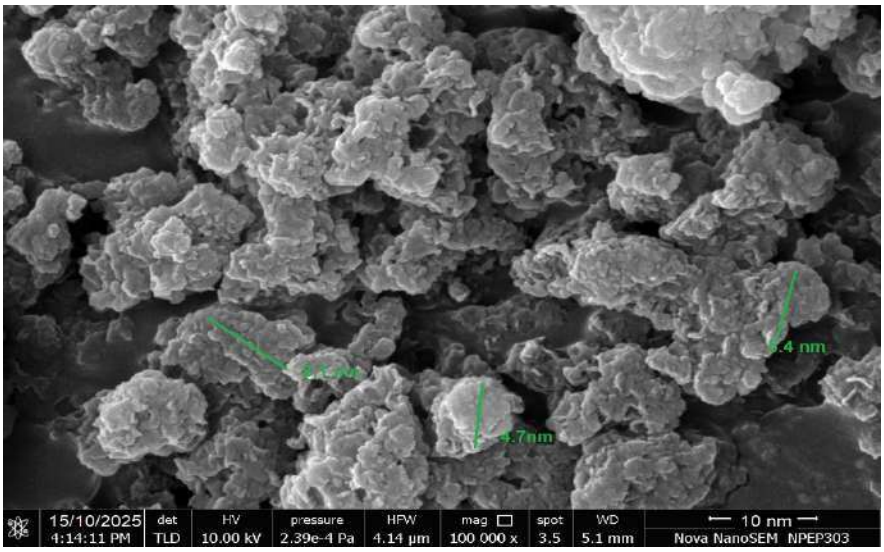

Fig 14: SEM of F6

Conclusion:

The SEM images of F6 show aggregated clusters of nanosized particles with irregular, roughly spherical shapes. Particle sizes range from 4.7–8.1 nm, confirming nanoscale dimensions. The rough, granular surface may enhance surface area for folic acid functionalization, and the absence of large agglomerates indicates uniform distribution and good structural stability.

7.5 Transmission Electron Microscopy (TEM) (JEOL, 2200FS)

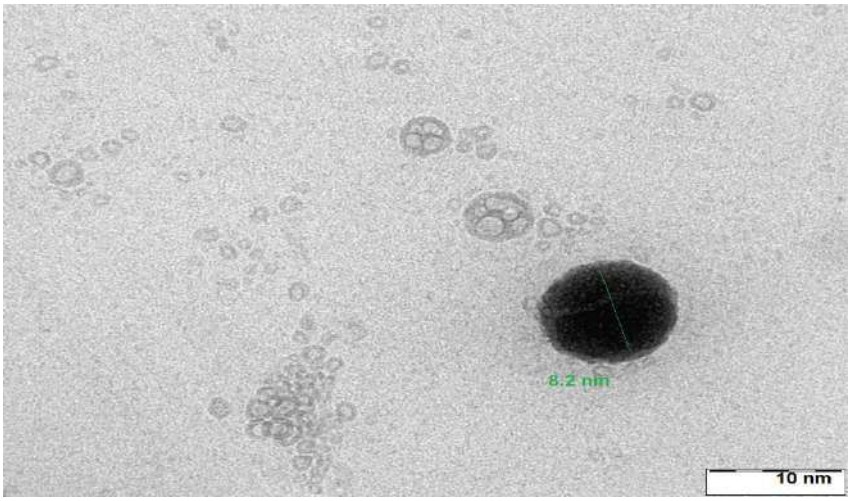

Fig 15: TEM of F6

Conclusion:

The TEM image of the F6 batch reveals well-defined, spherical nanoparticles with a uniform morphology. The average particle size is approximately 8.2 nm**,** as indicated by the scale measurement. The particles exhibit a smooth surface and monodisperse distribution, suggesting successful synthesis and stability of the nanostructure. The absence of significant aggregation further confirms good dispersibility and controlled particle formation, consistent with an efficient formulation process for folic acid-functionalized nanoparticles.

8. Results of Drug loaded Carbon dots of Nilotinib

8.1 DLS (particle size and zeta potential)

Table 5: Particle size of NF1 to NF9

Formulation code	Particle size (nm)	PDI	Zeta potential
NF1	7.18	0.248	-21.2
NF2	9.71	0.287	22.4
NF3	8.72	0.178	-18.2
NF4	8.5	0.121	-25.2
NF5	6.22	0.394	-23.4
NF6	9.11	0.316	-19.8
NF7	12.3	0.319	-14.5
NF8	10.4	0.286	-21.8
NF9	11.4	0.289	-23.4

Conclusion

All carbon dot formulations (NF1–NF9) were nanosized (6.22–12.3 nm) with acceptable PDI (0.121–0.394) and negative zeta potentials (–14.5 to –25.2 mV), indicating good size distribution and moderate stability. NF5 showed the smallest particle size (6.22 nm) with sufficient stability, making it the most promising batch for further applications.

ANOVA for Quadratic Model – Particle Size

The quadratic model is statistically significant ($F = 15.99$, $p = 0.0226$). Nilotinib (A) and its quadratic term (A^2) significantly influence particle size, indicating a strong nonlinear effect, while stirring speed and interaction terms are not significant. The model exhibits an excellent fit ($R^2 = 0.9638$) with good predictability and reliability.

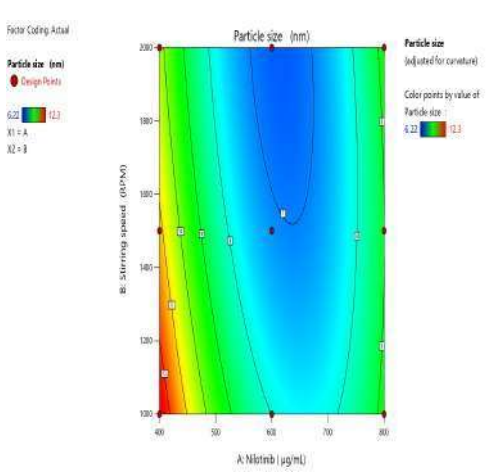

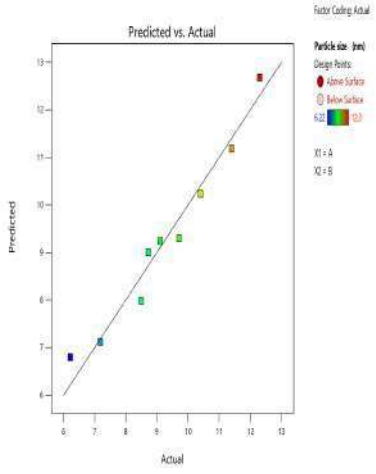

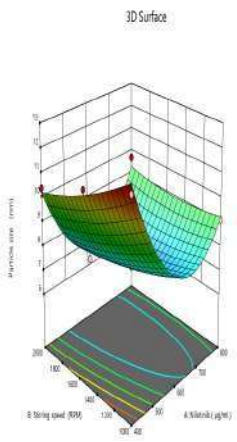

Fig 16: A **Fig 17: B** **Fig 18: C**

(Figure A: Counter Plot, Figure B: Predicted vs actual Plot, Figure C: 3D Surface Plot)

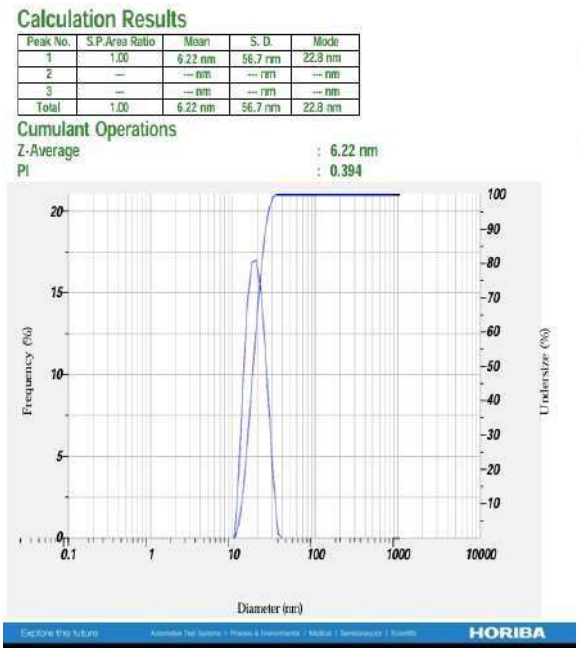

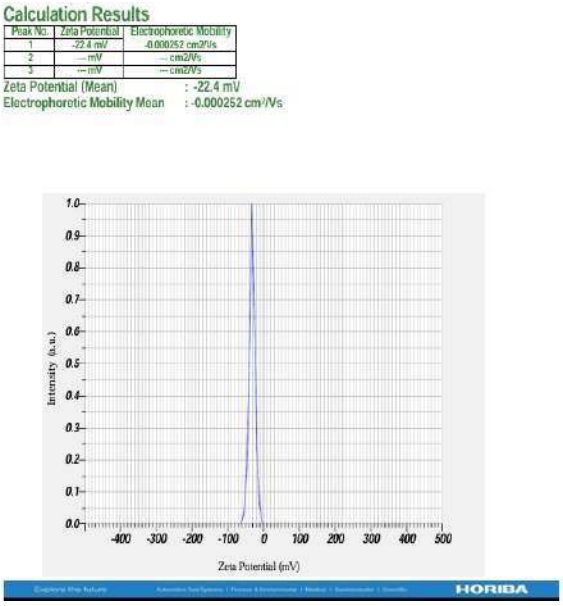

Fig 19: Particle size of NF5 **Fig 20: Zeta potential of NF5**

8.2 Drug content

Table 6: Drug content of NF1 to NF9

Formulation Code	Drug content (%)
NF1	93.02 ± 0.0028
NF2	88.94 ± 0.0001
NF3	84.25 ± 0.0025
NF4	88.27 ± 0.0017
NF5	96.37 ± 0.0007
NF6	86.35 ± 0.0011
NF7	84.49 ± 0.0023
NF8	94.87 ± 0.0018
NF9	86.59 ± 0.0018

Conclusion

All formulations (NF1–NF9) showed acceptable drug content, indicating uniform drug distribution. Among them, NF5 exhibited the highest drug content (96.37%), making it the optimized batch. The superior drug loading in NF5 suggests better entrapment efficiency and overall formulation stability compared to the other batches.

ANOVA for Quadratic Model – Drug Content

The quadratic model is statistically significant ($F = 11.75$, $p = 0.0348$). Stirring speed (B) and the quadratic term of Nilotinib (A^2) significantly influence drug content, while linear Nilotinib, interaction (AB), and B^2 are not significant. The model shows a strong fit ($R^2 = 0.9514$) with good predictability and reliability.

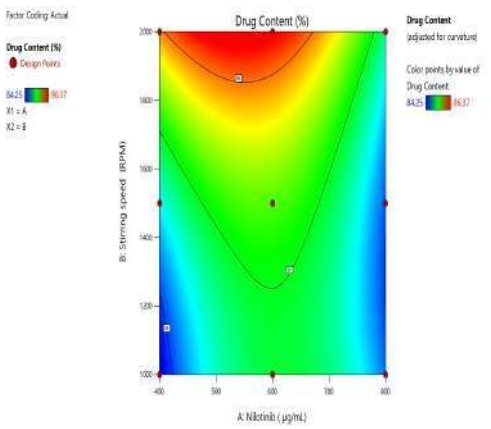

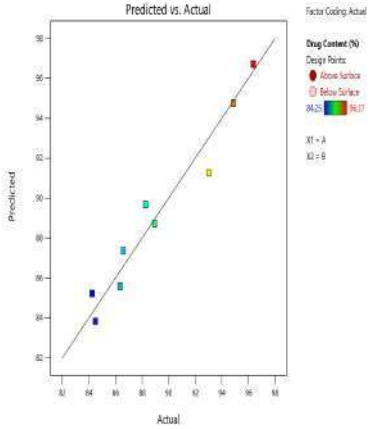

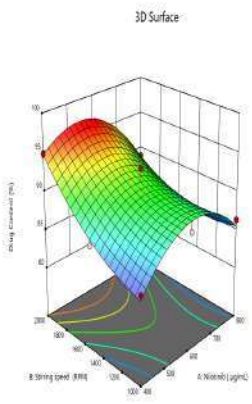

Fig 21: A **Fig 22: B** **Fig 23: C**

(Figure A: Counter Plot, Figure B: Predicted vs actual Plot, FigureC: 3D Surface Plot)

8.3 Encapsulation Effieciency

Table 7: Encapsulation Effieciency

Formulation Code	Encapsulation Effieciency (%)
NF1	85.96 ± 0.0014
NF2	82.19 ± 0.0025
NF3	82.66 ± 0.0087
NF4	82.60 ± 0.0004
NF5	88.27 ± 0.0009
NF6	85.17 ± 0.0001
NF7	78.12 ± 0.0028
NF8	86.12 ± 0.0010
NF9	80.73 ± 0.0037

Conclusion

The encapsulation efficiency of all formulations (NF1–NF9) ranged from moderate to high, indicating effective drug entrapment within the nanoparticle system. Among the batches, NF5 showed the highest encapsulation efficiency (88.27%), demonstrating superior drug loading capacity and overall formulation performance. In contrast, NF7 exhibited the lowest efficiency (78.12%), suggesting the need for further optimization. Based on these findings, NF5 can be considered the optimized formulation due to its maximum encapsulation efficiency.

ANOVA for Quadratic Model – Entrapment Efficiency

The quadratic model is statistically significant ($F = 9.39$, $p = 0.0473$). Stirring speed (B), the interaction term (AB), and the quadratic term of Nilotinib (A^2) significantly affect entrapment efficiency, while linear Nilotinib and B^2 are not significant. The model demonstrates a strong fit ($R^2 = 0.9399$) with good predictability and reliability.

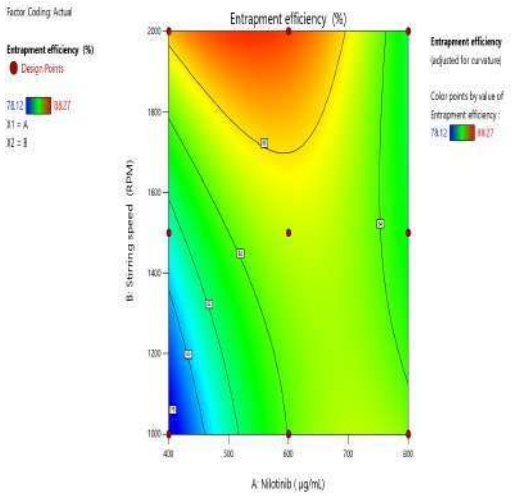

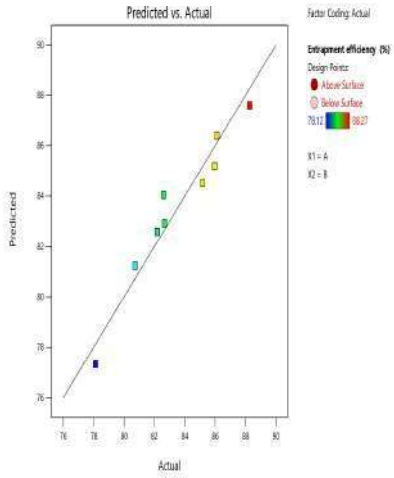

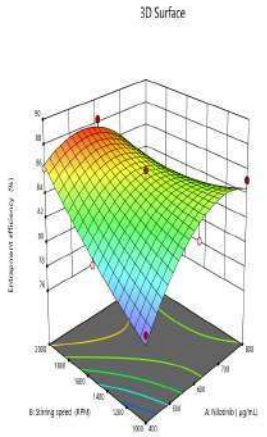

Fig 24: A **Fig 25: B** **Fig 26: C**

Figure A: Counter Plot, Figure B: Predicted vs actual Plot, Figure C: 3D Surface Plot

8.4 Dissolution studies

Table 8: In vitro drug release of NF1 to NF9

Time in (HR)	NF1	NF2	NF3	NF4	NF5	NF6	NF7	NF8	NF9
0	0	0	0	0	0	0	0	0	0
1	6.16 ± 0.0012	5.46 ± 0.032	3.78 ± 0.0001	7.28 ± 0.0006	10.64 ± 0.0047	4.62 ± 0.0018	3.36 ± 0.0038	2.52 ± 0.0674	4.20 ± 0.0258
2	14.57 ± 0.0036	11.34 ± 0.0078	9.24 ± 0.0005	15.69 ± 0.0017	20.17 ± 0.0048	7.56 ± 0.0064	10.08 ± 0.0125	9.24 ± 0.0369	10.92 ± 0.0247
3	20.17 ± 0.0034	17.65 ± 0.0941	15.97 ± 0.0048	21.29 ± 0.0048	26.89 ± 0.0036	14.71 ± 0.0006	17.65 ± 0.0625	16.81 ± 0.0147	18.49 ± 0.0036
4	27.45 ± 0.0001	24.79 ±0.0003	23.11 ± 0.0017	28.01 ± 0.0028	35.29 ± 0.0014	21.43 ± 0.0038	24.37 ± 0.0068	23.53 ± 0.0369	25.21 ± 0.0048
5	35.85 ± 0.0014	32.35 ± 0.0087	30.25 ± 0.0091	36.97 ± 0.0036	43.70 ± 0.0087	26.89 ± 0.0001	29.41 ± 0.0062	29.41 ± 0.0147	30.25 ± 0.0018
6	47.06 ± 0.0014	37.39 ± 0.0741	35.71 ± 0.0031	48.18 ± 0.0019	54.90 ± 0.0094	34.03 ± 0.0152	35.29 ± 0.0014	34.45 ± 0.0147	36.13 ± 0.0241
7	54.34 ± 0.0011	41.60 ± 0.0018	39.50 ±0.0087	55.46 ± 0.0074	61.06 ± 0.0037	39.08 ± 0.0357	47.06 ± 0.0123	46.22 ± 0.0369	47.90 ± 0.0258
8	59.94 ± 0.0074	55.04 ± 0.0003	52.10 ± 0.0010	61.06 ± 0.0030	67.79 ± 0.0036	47.90 ± 0.0624	53.78 ± 0.0674	52.94 ± 0.0357	54.62 ± 0.0147
9	71.15 ± 0.0140	61.34 ± 0.0074	59.24 ± 0.0026	72.27 ± 0.0018	74.51 ± 0.0074	54.20 ± 0.0068	59.66 ± 0.0648	58.82 ± 0.0159	60.50 ± 0.0158
10	77.31 ± 0.0017	78.99 ± 0.0097	69.33 ± 0.0018	78.43 ± 0.0016	79.55 ± 0.0017	59.24 ± 0.0084	69.75 ± 0.4982	68.91 ± 0.0258	70.59 ± 0.0361
11	83.47 ± 0.0048	84.45 ± 0.0048	79.41 ± 0.0018	85.15 ± 0.0087	86.83 ± 0.0016	76.89 ± 0.0016	80.67 ± 0.0037	79.83 ± 0.0358	80.67 ± 0.0004
12	88.52 ±0.0019	92.02 ± 0.0194	89.92 ± 0.0049	93.56 ± 0.0047	96.92 ± 0.0049	87.82 ± 0.0039	91.60 ± 0.0147	90.76 ± 0.0257	92.44 ± 0.0018

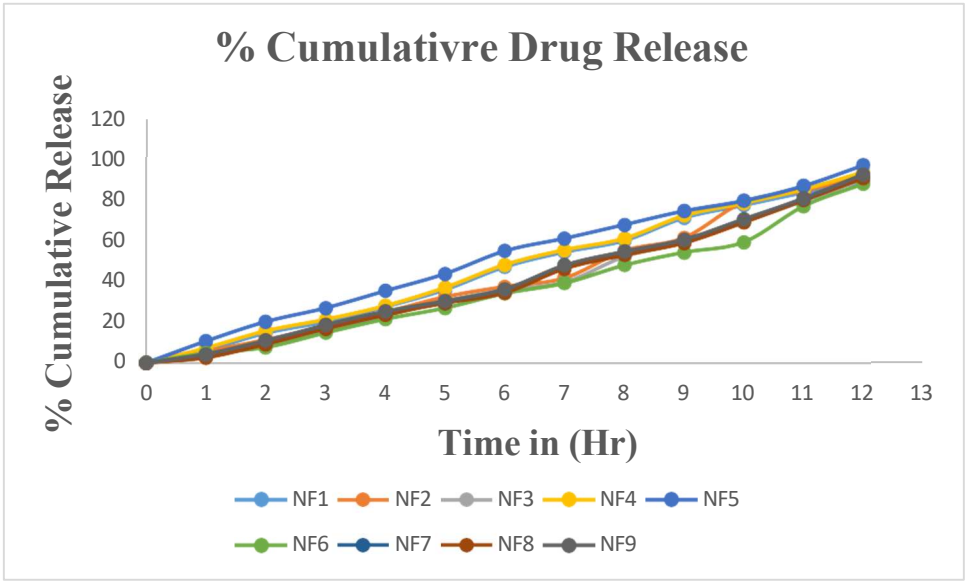

Fig 27: % Drug release from NF1-NF9

Conclusion

All formulations (NF1–NF9) show a time-dependent increase in drug release, with very low release at 0 hr and gradual increase over 12 hr. NF5 exhibits the fastest and highest drug release (96.92% at 12 hr), indicating superior dissolution. NF2, NF4, NF9, and NF8 also show high release (>90% by 12 hr), while NF1, NF3, NF6, and NF7 have slightly slower release. Overall, the data suggest efficient in vitro drug release for all formulations, with differences reflecting varying formulation characteristics.

8.5 FTIR

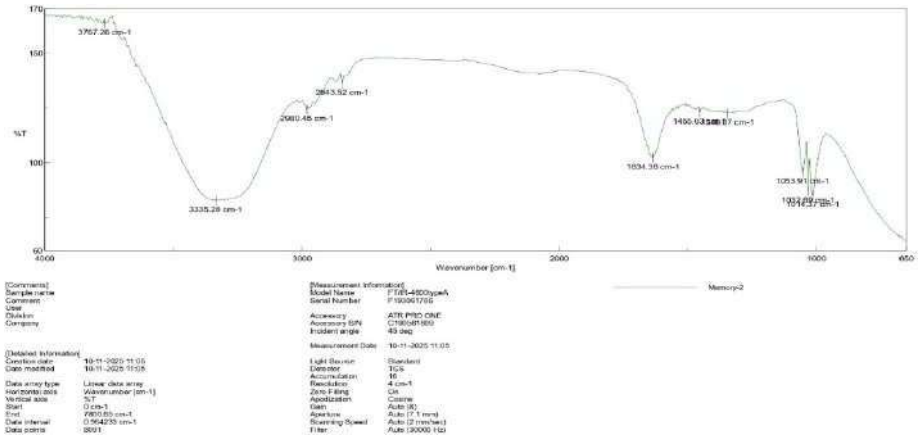

Fig 28: FTIR of NF5

Conclusion

The FTIR spectrum of NF5 shows characteristic peaks for O–H/N–H, C–H, C=O, and C–O groups. A broad band at 3335 cm^{-1} indicates hydrogen bonding, and the shifted carbonyl peak at 1634 cm^{-1} suggests strong interactions between Nilotinib, carbon dots, and the cellulose acetate matrix. The presence of polymer (C–O–C) and drug (C–N, aromatic C–H) bands confirms successful encapsulation of Nilotinib without chemical degradation.

8.6 DSC

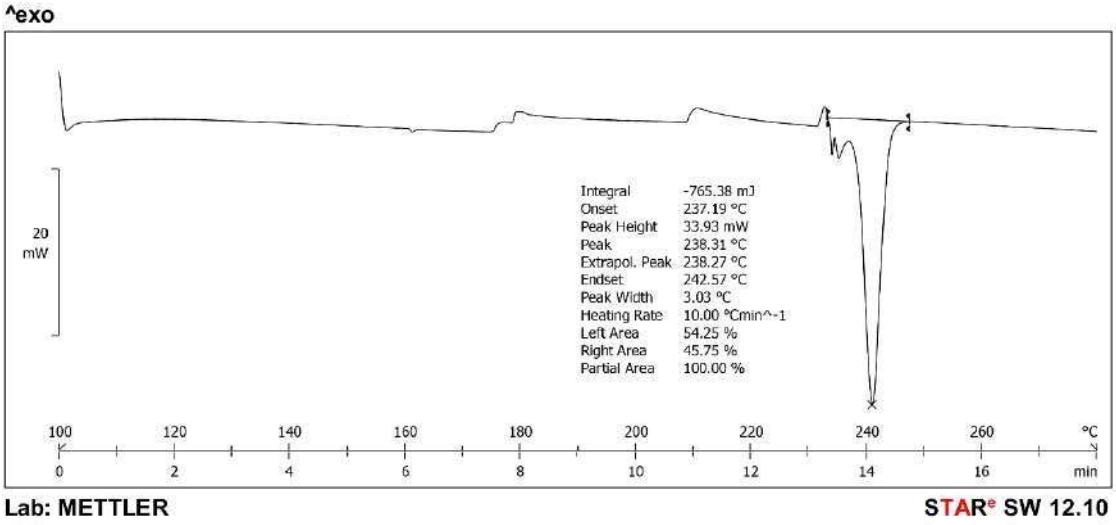

Fig 29: DSC of NF5

Conclusion:

A peak at approximately 238.31 °C in a Differential Scanning Calorimetry (DSC) graph of a nilotinib co-crystal most likely indicates an endothermic event, specifically the melting point (233) of the specific co-crystal form or a new crystalline polymorph.

8.7 Raman Analysis

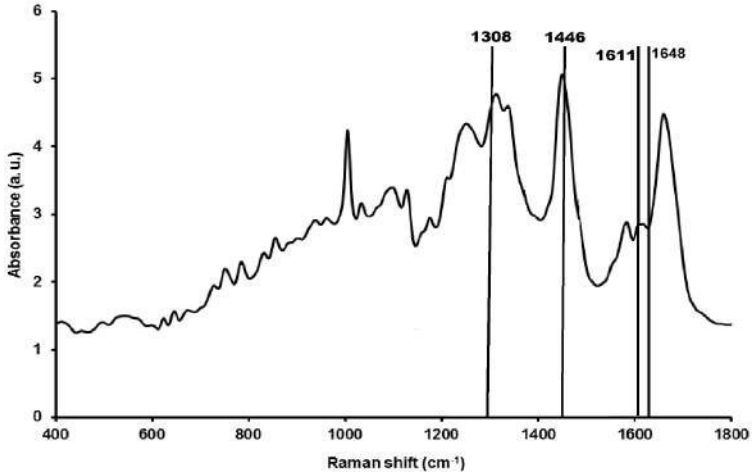

Fig 30: Raman analysis

Conclusion

Raman spectroscopy is mainly reported for identifying nilotinib itself or its co-crystal forms, rather than nilotinib–carbon dot composites. Characteristic Raman peaks at ~1648, 1611, 1446, and 1308 cm^{-1} correspond to amide/ring stretching, aromatic C=C stretching, CH_2/CH_3 deformation, and C–N/C–C stretching, confirming the crystalline structure and hydrogen-bonding environment of nilotinib.

8.9 Fluorescence spectroscopy

8.9.1 NF5

Dilutions	Blue	Green

Control	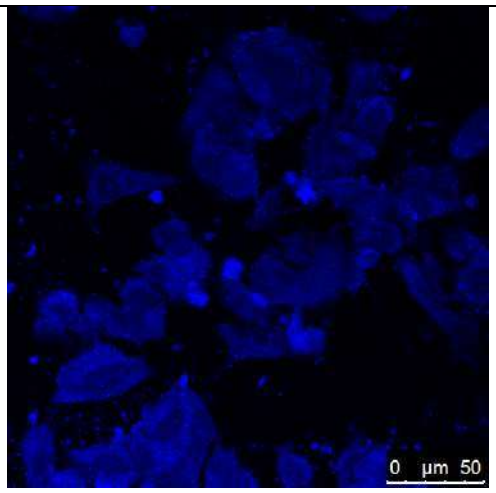	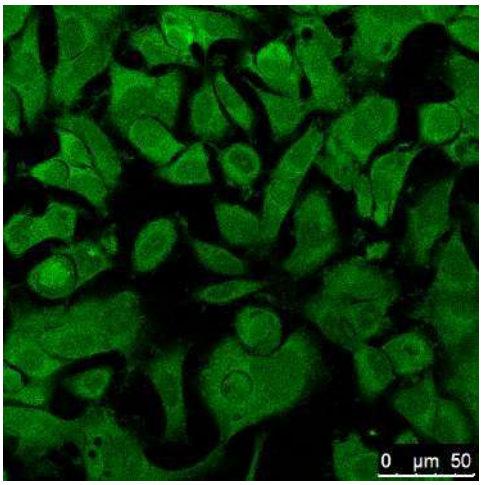
10	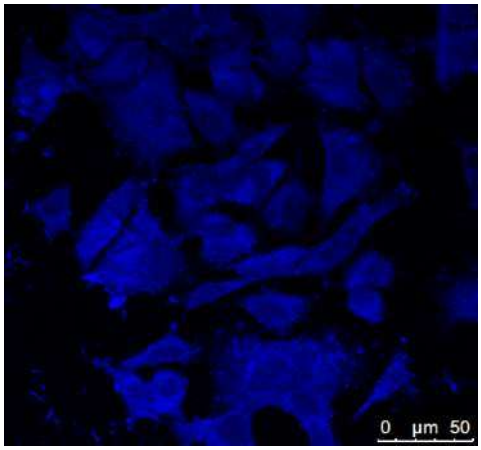	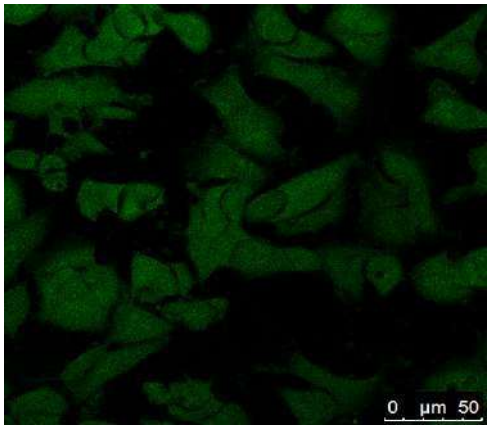
50	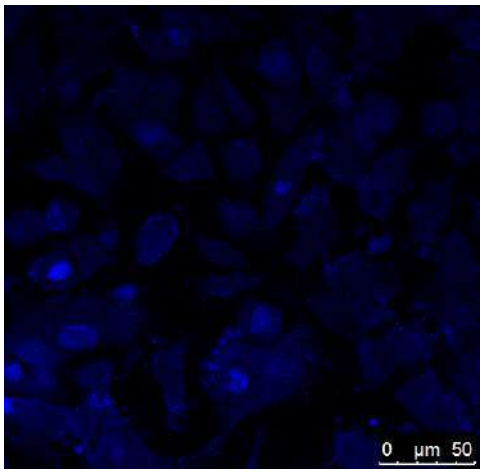	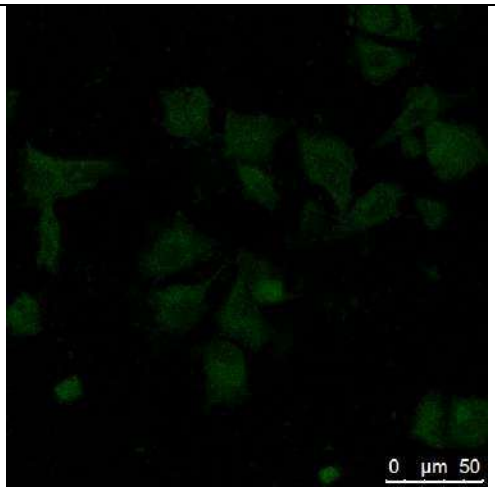

Fig 31: Morphological Observations of NF5 Treated Wells

Table 9: Morphological Observations of NF5

Sr.no	Count	Total Area	Average Size	%Area	Mean
10 blue	1012	4.241	0.005	8.178	24.47
10 green	198	6.415	0.031	12.457	27.085
50 blue	4564	7.255	0.002	14.125	19.47
50 green	912	7.745	0.008	15.352	23.54

Conclusion

In the above study, Hoechst 3334 and Calcein-AM fluorescent stains demonstrated that the NF5 promoted apoptosis and to a lesser degree, necrosis-driven cell death in A549 breast cancer cells.

8.10 Quantum yield

8.11 TEM

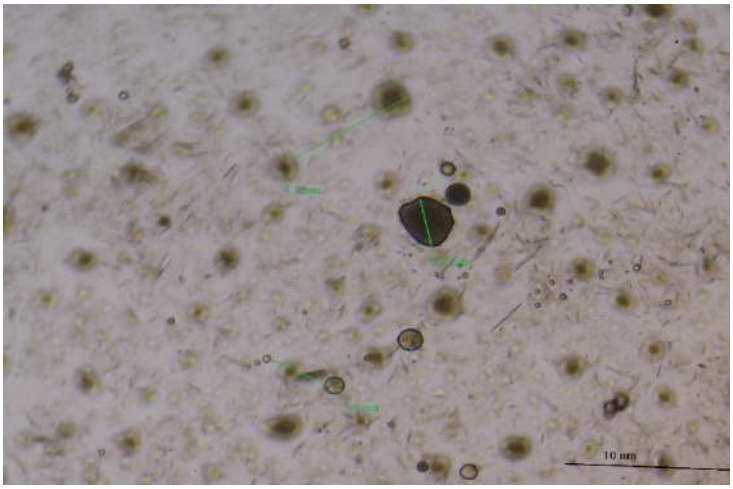

Fig 32: TEM of optimized formulation NF5

Conclusion

TEM images of NF5 show well-defined, nearly spherical nanoparticles sized 4.3–8.8 nm, confirming nanoscale dimensions. The particles are uniformly dispersed with minimal aggregation, exhibiting smooth surfaces and consistent size, indicating good colloidal stability and successful synthesis of Nilotinib-loaded carbon dots.

8.12 XRD

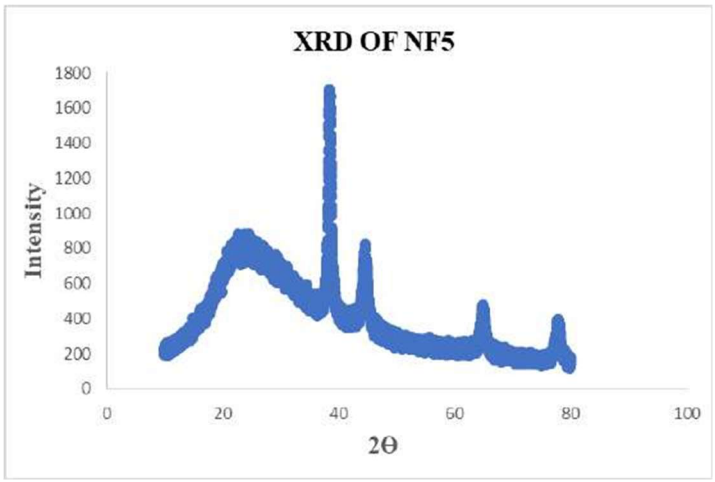

Fig 33: XRD of NF5

Conclusion

The XRD pattern suggests that Nilotinib, when incorporated into the carbon dot carrier, has lost its crystalline characteristics and has transformed into an amorphous or molecularly dispersed form within the matrix. This amorphization typically enhances drug solubility and dissolution rate, which is beneficial for poorly soluble drugs like Nilotinib.

8.13 In-vitro cytotoxicity (Cell line study) by using human adenocarcinoma cell line (A549)

NF5 (Optimized formulation)

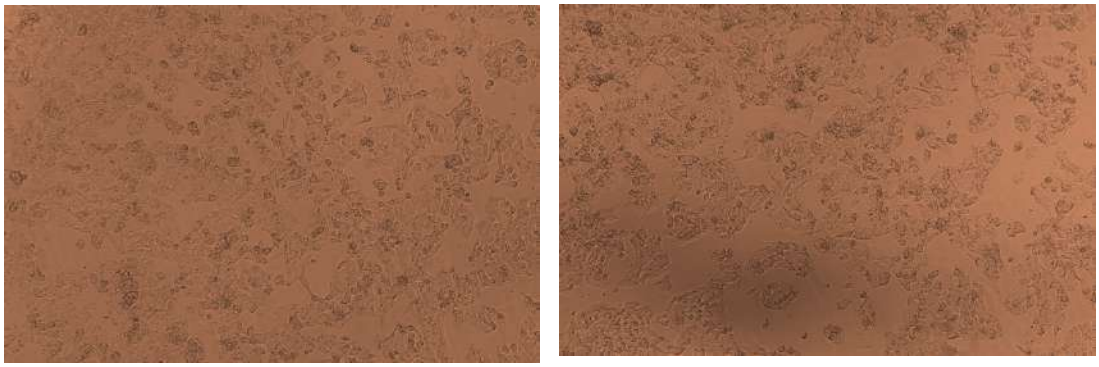

Fig 34:

Morphological Observations of Control Well of NF5

Dilutions	NF5 (0 hr)	NF5 (24 hrs)
1 µl/mL	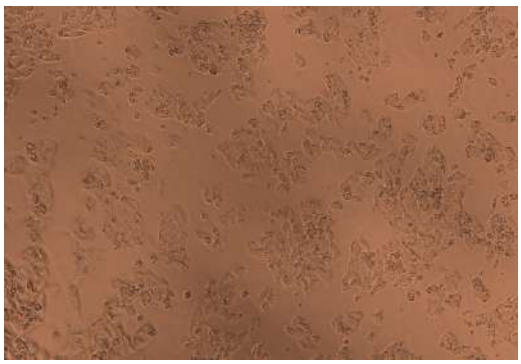	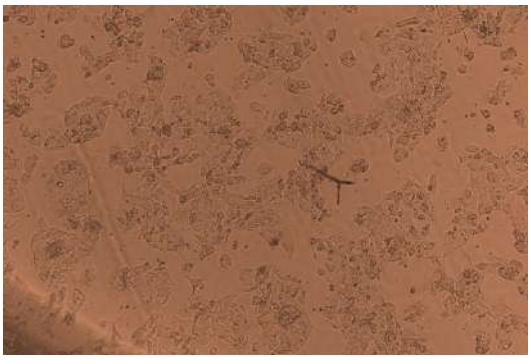

5 µl/mL	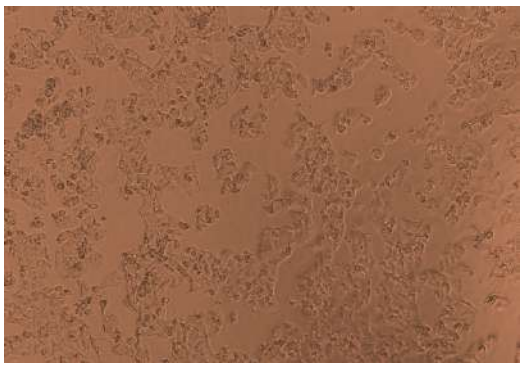	
10 µl/mL		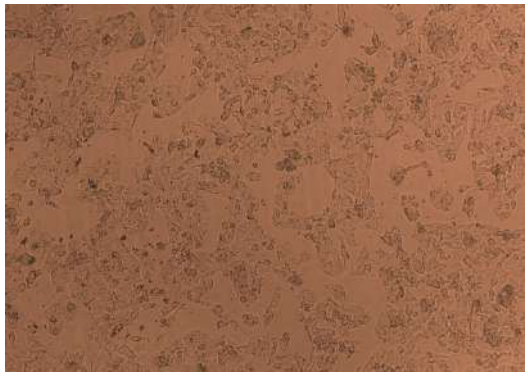
25 µl/mL		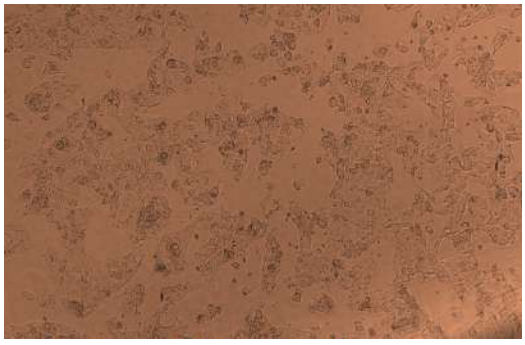
50 µl/mL		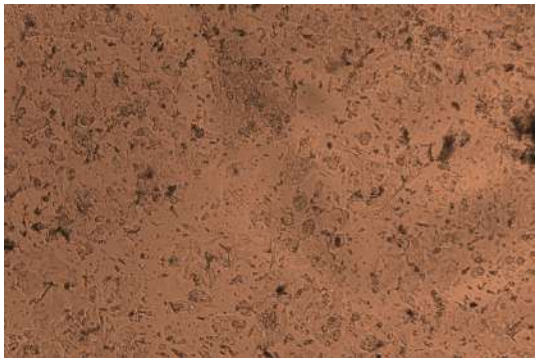

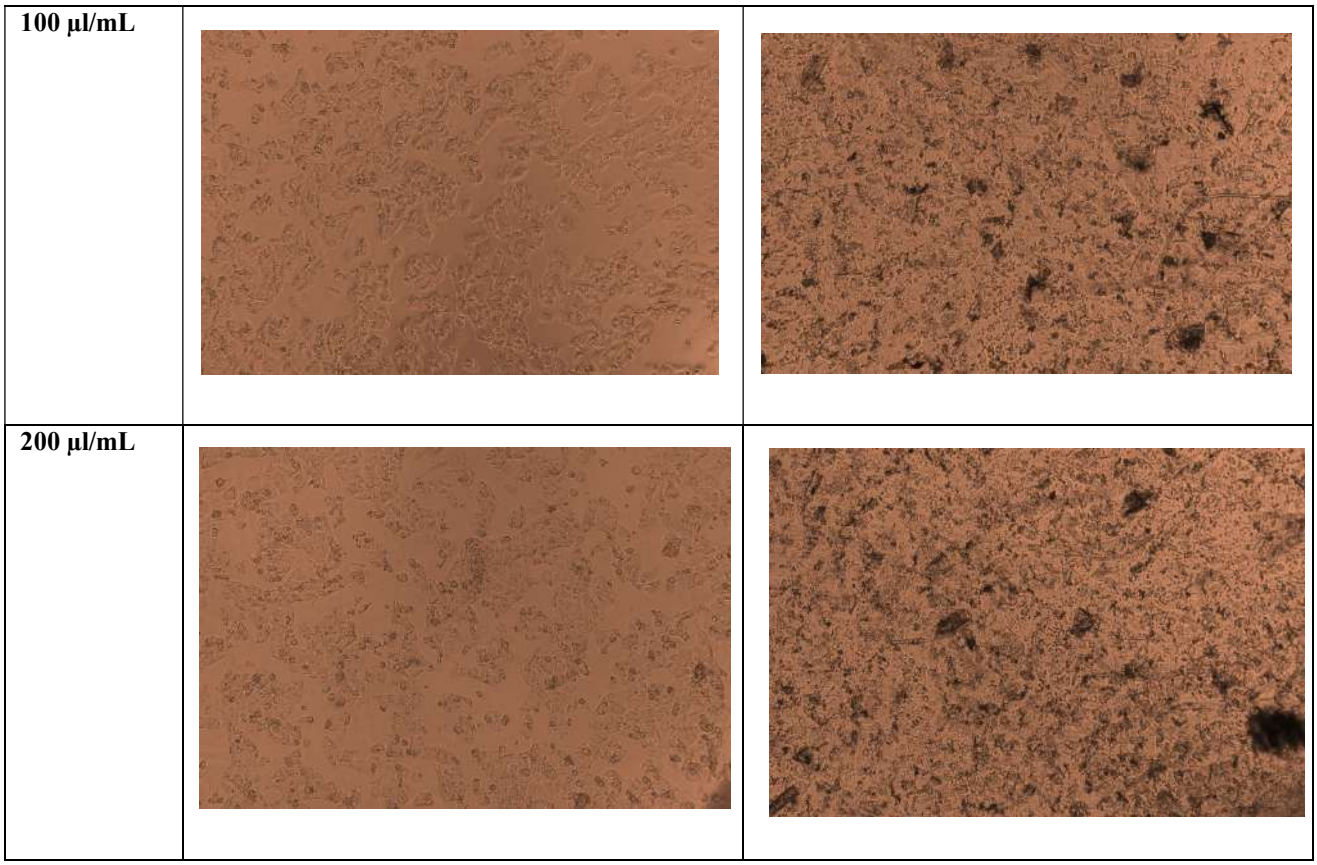

Fig 35: Morphological Observations of NF5 Treated Wells

Table 10: MTT Results: NF5

CTRL/ CONC.		1	5	10	25	50	100	200
R1	1.221	1.187	1.174	0.987	0.678	0.741	0.578	0.487
R2	1.339	1.006	0.874	0.871	0.771	0.536	0.512	0.541
R3	1.624	0.987	0.787	0.741	0.745	0.451	0.436	0.433
Mean Absorbance	1.395	1.060	0.945	0.866	0.731	0.576	0.509	0.487

Table 11

CONC.	Control	1	5	10	25	50	100	200
% Cell Survival	87.5478	85.10994	84.17782	70.7696	48.61377	53.13097	41.44359	34.91874
	96.0086	72.13193	62.6673	62.4522	55.28203	38.43212	36.71128	38.79063
	116.4436	70.7696	56.42925	53.13097	53.41778	32.33748	31.26195	31.04684
Average % Cell Survival	**100**	**76.00382**	**67.75813**	**62.11759**	**52.43786**	**41.30019**	**36.47227**	**34.91874**
IC50								

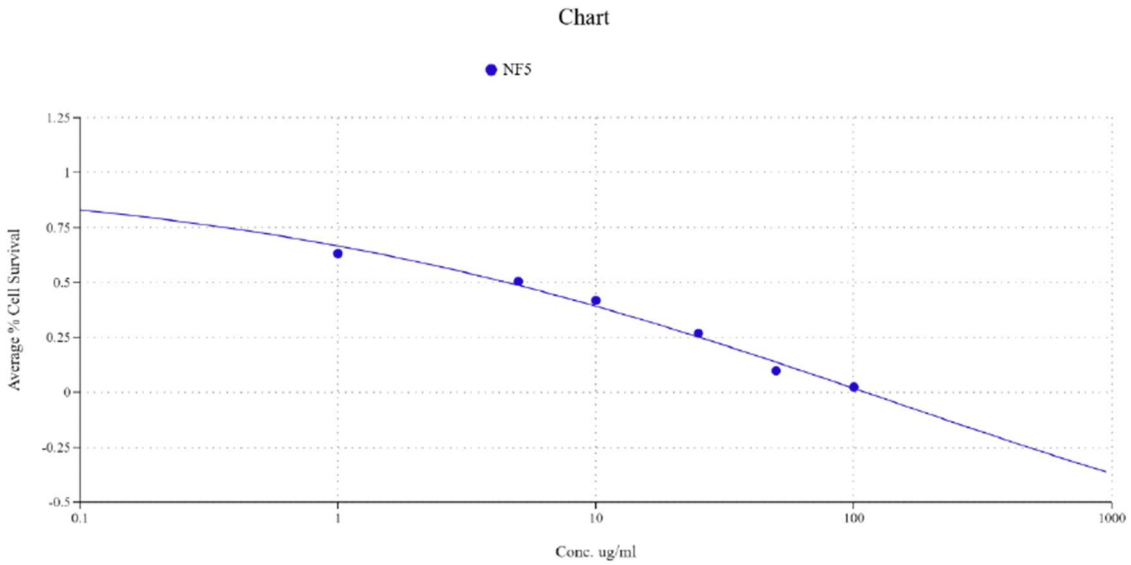

Fig 36: Graph of conc vs % cell Viability- NF5

2. Nilotinib pure drug

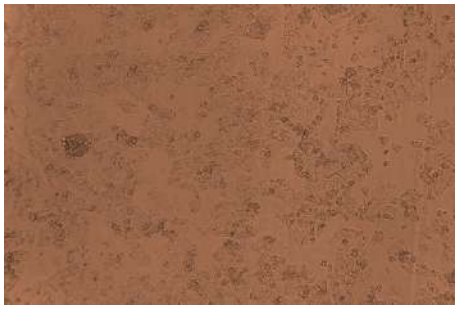
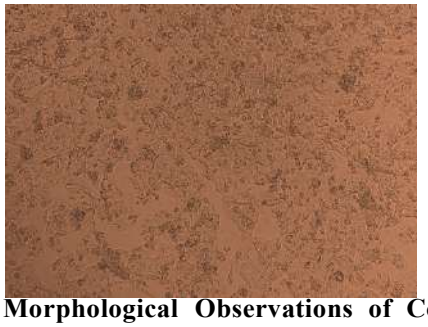

Fig 37: Morphological Observations of Control Well of Nilotinib

Dilutions	Nilotinib (0 hr)	Nilotinib (24 hrs)
1 µl/mL	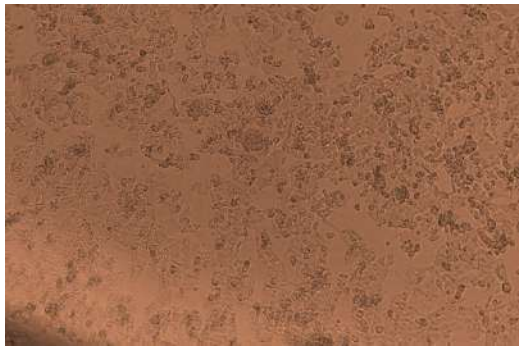	

5 µl/mL	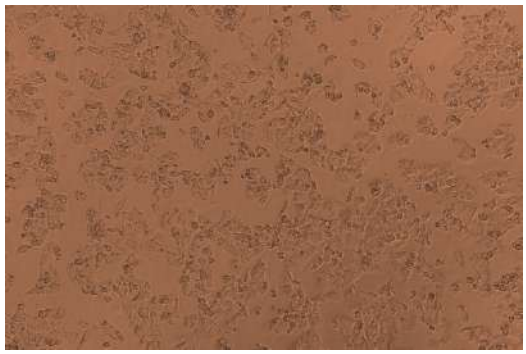	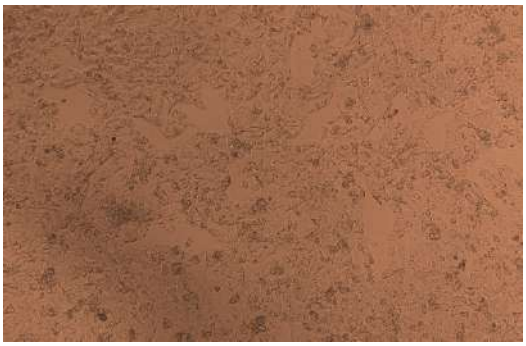
10 µl/mL	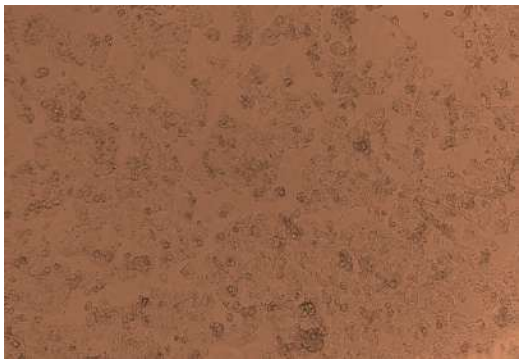	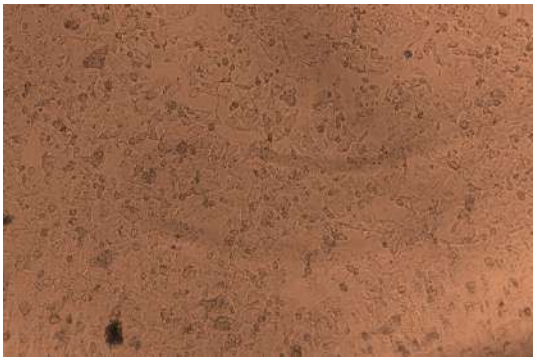
25 µl/mL	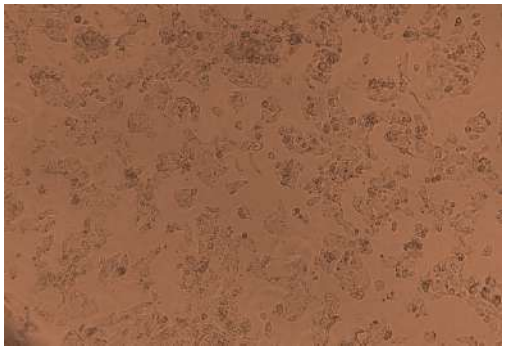	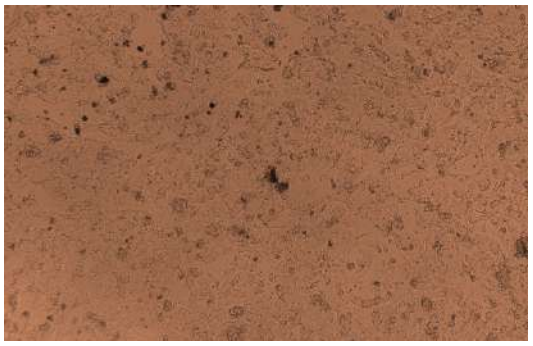
50 µl/mL	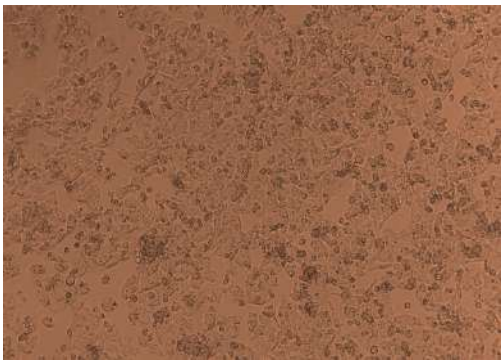	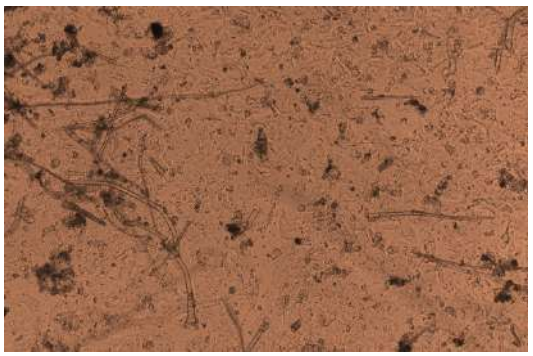

100 µl/mL	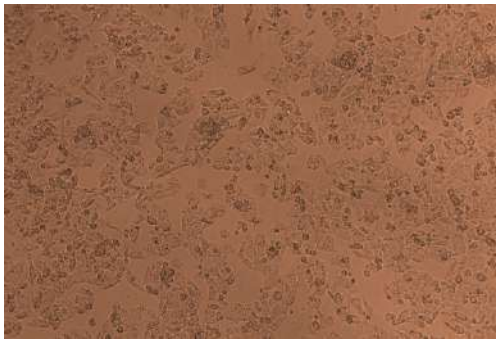	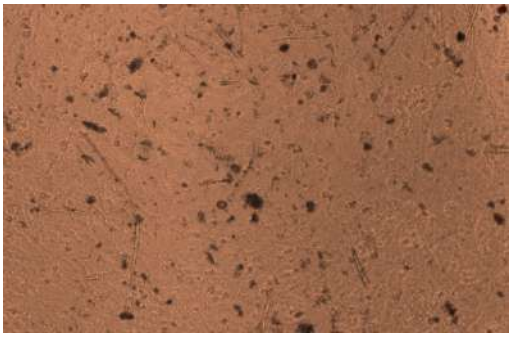
200 µl/mL	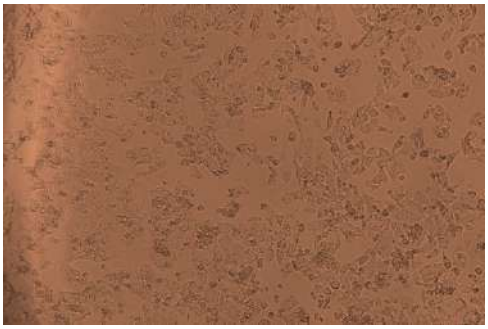	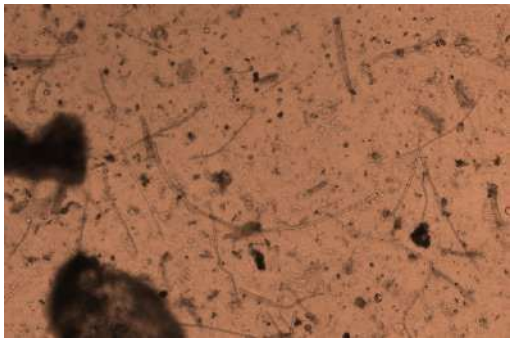

Fig 38: Morphological Observations of Nilotinib Treated Wells

Table 12: MTT Results: Nilotinib pure drug

CTRL/ CONC.		**1**	**5**	**10**	**25**	**50**	**100**	**200**
R1	1.535	1.245	1.245	1.121	1.047	1.321	1.214	0.974
R2	1.747	1.341	1.321	1.024	1.003	0.978	0.654	0.621
R3	1.942	1.452	1.115	1.365	1.247	0.841	0.489	0.452
Mean Absorbance	1.741	1.346	1.227	1.170	1.099	1.047	0.786	0.682

Table 13

CONC.	**Control**	**1**	**5**	**10**	**25**	**50**	**100**	**200**
% Cell Survival	88.15084	71.49694	71.49694	64.37596	60.12634	75.86141	69.71669	55.93415
	100.3254	77.00996	75.86141	58.80551	57.59954	56.16386	37.55743	35.66233
	111.5237	83.38438	64.03139	78.38821	71.61179	48.29633	28.08193	25.95712
Average % Cell Survival	**100**	**77.29709**	**70.46325**	**67.18989**	**63.11256**	**60.1072**	**45.11868**	**39.18453**
IC50	**235.1168**							

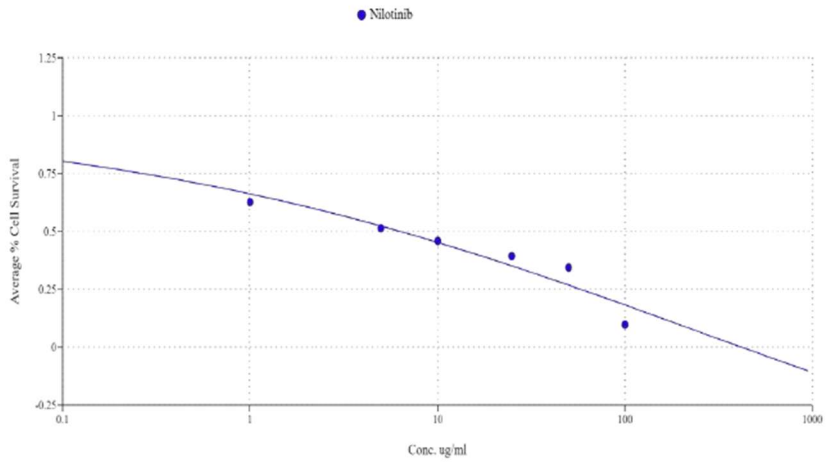

Fig 39: Graph of conc vs % cell Viability- Nilotinib pure drug

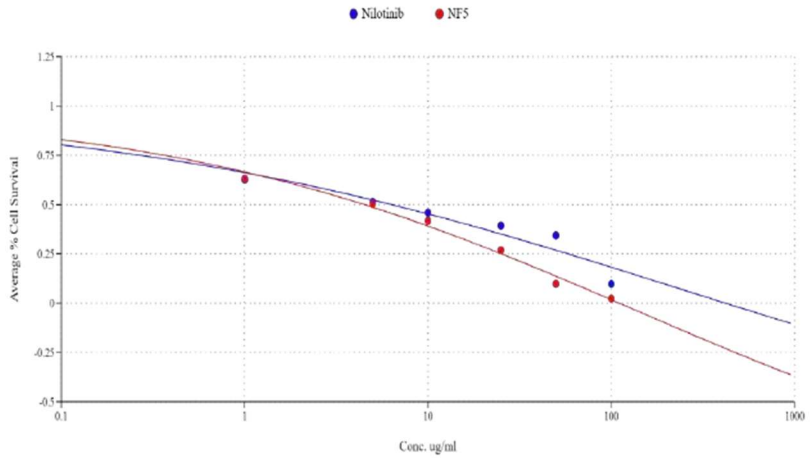

Fig 40: Comparative Graph of conc vs % cell Viability- CF7 Vs Nilotinib pure drug

Table 14 : IC50 values of MTT Assay

Sr. No.	Test Item	Log IC50 Value
1.	**NF5**	133.7971
2.	**Nilotinib pure drug**	235.1168

Conclusion

The Log IC50 values must be converted to the IC50 concentration to understand the actual potency of each test item. The IC50 is calculated using the formula: $IC_{50} = 10^{\text{Log}IC50}$

Table 15: Log IC50 and IC50

Sr. No.	Test Item	Log IC50	IC50 (µg/mL)
1	NF5	133.7971	6.27×10^{133}
2	Nilotinib pure drug	235.1168	1.31×10^{235}

With a lower Log $IC50$ (133.7971) compared to Nilotinib (235.1168), NF5 is the more potent agent. It requires a lower concentration to inhibit 50% of cell growth.

CONCLUSION

The potential of folic acid-functionalized carbon dots as an effective nanocarrier system for Nilotinib targeted distribution is well demonstrated by this study. The modified formulation NF5 demonstrated improved in vitro anticancer activity, high drug loading, prolonged release, nanoscale size, and good stability. Effective encapsulation, drug amorphization, and molecular integrity preservation were verified by structural and thermal investigations. The intrinsic fluorescence of carbon dots and the enhanced cytotoxicity and apoptosis-inducing potential of NF5 underscore its appropriateness for theranostic uses in cancer therapy. All things considered, the proposed nanocarrier technology presents a viable approach to overcoming Nilotinib's solubility and bioavailability restrictions and offers a solid basis for more in vivo and clinical research in targeted anticancer therapy.

CONFLICT OF INTEREST

None, declared by authors.

REFERENCES

1. Hassanpour SH, Dehghani M. Review of cancer from perspective of molecular. Journal of cancer research and practice. 2017 Dec 1;4(4):127-9.
2. Siegel RL, Miller KD, Wagle NS, Jemal A. Cancer statistics, 2023. CA: a cancer journal for clinicians. 2023 Jan 1;73(1).
3. Gm C. The cell: a molecular approach. Sunderland (MA): Sinauer Associates. 2000:3.
4. Hanahan D. Hallmarks of cancer: new dimensions. Cancer discovery. 2022 Jan 1;12(1):31-46.
5. Majcherek D, Weresa MA, Ciecierski C. A cluster analysis of risk factors for Cancer across EU countries: health policy recommendations for prevention. International Journal of Environmental Research and Public Health. 2021 Jul 31;18(15):8142.
6. Barsouk A, Thandra KC, Saginala K, Rawla P, Barsouk A. Chemical risk factors of primary liver cancer: an update. Hepatic Medicine: Evidence and Research. 2021 Jan 5:179-88.
7. Holland JF. Holland-Frei cancer medicine 8. PMPH-USA; 2010.
8. Sarthi S, Bhardwaj H, Jangde RK. Recent Progress in Nanoemulsion Technology for the Management of Hepatic Diseases. Current Nanomedicine. 2024 Sep 25.
9. Sochacka-Ćwikła A, Mączyński M, Regiec A. FDA-approved drugs for hematological malignancies—the last decade review. Cancers. 2021 Dec 24;14(1):87.
10. Blum RH, Carter SK. Adriamycin: a new anticancer drug with significant clinical activity. Annals of internal medicine. 1974 Feb 1;80(2):249-59.
11. Rowinsky EK, Onetto N, Canetta RM, Arbuck S. Taxol: the first of the taxanes, an important new class of antitumor agents. InSeminars in oncology 1992 Dec 1 (Vol. 19, No. 6, pp. 646-662).
12. Cheng Z, Li M, Dey R, Chen Y. Nanomaterials for cancer therapy: current progress and perspectives. Journal of hematology & oncology. 2021 May 31;14(1):85.
13. Schirrmacher V. From chemotherapy to biological therapy: A review of novel concepts to reduce the side effects of systemic cancer treatment. International journal of oncology. 2019 Feb 1;54(2):407-19.
14. Dogra R, Bhatia R, Shankar R, Bansal P, Rawal RK. Enasidenib: first mutant IDH2 inhibitor for the treatment of refractory and relapsed acute myeloid leukemia. Anti-Cancer Agents in Medicinal Chemistry-Anti-Cancer Agents). 2018 Nov 1;18(14):1936-51.
15. Liu GH, Chen T, Zhang X, Ma XL, Shi HS. Small molecule inhibitors targeting the cancers. MedComm. 2022 Dec;3(4):e181.
16. Marei HE, Cenciarelli C, Hasan A. Potential of antibody–drug conjugates (ADCs) for cancer therapy. Cancer Cell International. 2022 Aug 13;22(1):255.
17. Arruebo M, Vilaboa N, Sáez-Gutierrez B, Lambea J, Tres A, Valladares M, González-Fernández Á. Assessment of the evolution of cancer treatment therapies. Cancers. 2011 Aug 12;3(3):3279-330.
18. Lu W, Lieber CM. Semiconductor nanowires. Journal of Physics D: Applied Physics. 2006 Oct 20;39(21):R387.

19. Yu DG, Zhu LM, White K, Branford-White C. Electrospun nanofiber-based drug delivery systems. Health. 2009 Sep 28;1(02):67.

20. Bianco A, Kostarelos K, Prato M. Applications of carbon nanotubes in drug delivery. Current opinion in chemical biology. 2005 Dec 1;9(6):674-9.

21. Danaei MR, Dehghankhold M, Ataei S, Hasanzadeh Davarani F, Javanmard R, Dokhani A, Khorasani S, Mozafari YM. Impact of particle size and polydispersity index on the clinical applications of lipidic nanocarrier systems. Pharmaceutics. 2018 May 18;10(2):57.

22. Karavas E, Georgarakis M, Docoslis A, Bikiaris D. Combining SEM, TEM, and micro-Raman techniques to differentiate between the amorphous molecular level dispersions and nanodispersions of a poorly water-soluble drug within a polymer matrix. International journal of pharmaceutics. 2007 Aug 1;340(1-2):76-83.

23. Filippov SK, Khusnutdinov R, Murmiliuk A, Inam W, Zakharova LY, Zhang H, Khutoryanskiy VV. Dynamic light scattering and transmission electron microscopy in drug delivery: A roadmap for correct characterization of nanoparticles and interpretation of results. Materials Horizons. 2023;10(12):5354-70.

24. Yuan Y, Guo B, Hao L, Liu N, Lin Y, Guo W, Li X, Gu B. Doxorubicin-loaded environmentally friendly carbon dots as a novel drug delivery system for nucleus targeted cancer therapy. Colloids and Surfaces B: Biointerfaces. 2017 Nov 1;159:349-59.

25. Smerikarova M, Bozhanov S, Maslarska V. Development of HPLC-UV method for determination of Nilotinib in spiked human plasma with greenness assessment. Microchemical Journal. 2024 Dec 1;207:112220.

26. Ivaturi RA, Sastry TM, Satyaveni S. Development and validation of a stability indicating HPLC method for the determination of nilotinib hydrochloride in bulk and pharmaceutical dosage form. Int. J. Pharm. Pharm. Sci. 2016;8(9):41.

27. Fawaz W, Hanano A, Murad H, Yousfan A, Alghoraibi I, Hasian J. Polymeric nanoparticles loaded with vincristine and carbon dots for hepatocellular carcinoma therapy and imaging. Scientific Reports. 2024 Oct 18;14(1):24520.

28. Al-Musawi, S. et al. Smart nanoformulation based on polymeric magnetic nanoparticles and vincristine drug: A novel therapy for apoptotic gene expression in tumors. Life 11, 1–12 (2021).

29. Rajender G, Giri PK. Formation mechanism of graphene quantum dots and their edge state conversion probed by photoluminescence and Raman spectroscopy. Journal of Materials Chemistry C. 2016;4(46):10852-65.

30. Liao S, Zhao X, Zhu F, Chen M, Wu Z, Yang H, Chen X. Novel S, N-doped carbon quantum dot-based" off-on" fluorescent sensor for silver ion and cysteine. Talanta. 2018 Apr 1;180:300-8.

31. De M, Ghosh PS, Rotello VM. Applications of nanoparticles in biology. Advanced Materials. 2008 Nov 18;20(22):4225-41.

32. Zhang R, Chen X, Cheng Y, Chen Z, Li X, Deng Y. Recent advances of nanomaterials for intervention in Parkinson's disease in the context of anti-inflammation. Coordination Chemistry Reviews. 2024 Mar 1;502:215616.

33. He M, Zhang J, Wang H, Kong Y, Xiao Y, Xu W. Material and optical properties of fluorescent carbon quantum dots fabricated from lemon juice via hydrothermal reaction. Nanoscale Research Letters. 2018 Dec;13(1):175.

34. Eranikkal N, Riyamol KR, Shafaf H, Nawshad M, Maurya MR, Hasan A, Das P, Sadasivuni KK. Microwave-Assisted Synthesis of Nitrogen-Doped Carbon Dots for Sensitive Fluorescence-Based Urea Detection in Soil. Journal of Fluorescence. 2025 Jun 24:1-2.

35. Martindale, B.C.M.; Hutton, G.A.M.; Caputo, C.A.; Reisner, E. Solar Hydrogen Production Using Carbon Quantum Dots and a Molecular Nickel Catalyst. J. Am. Chem. Soc. 2015, 137, 6018–6025.